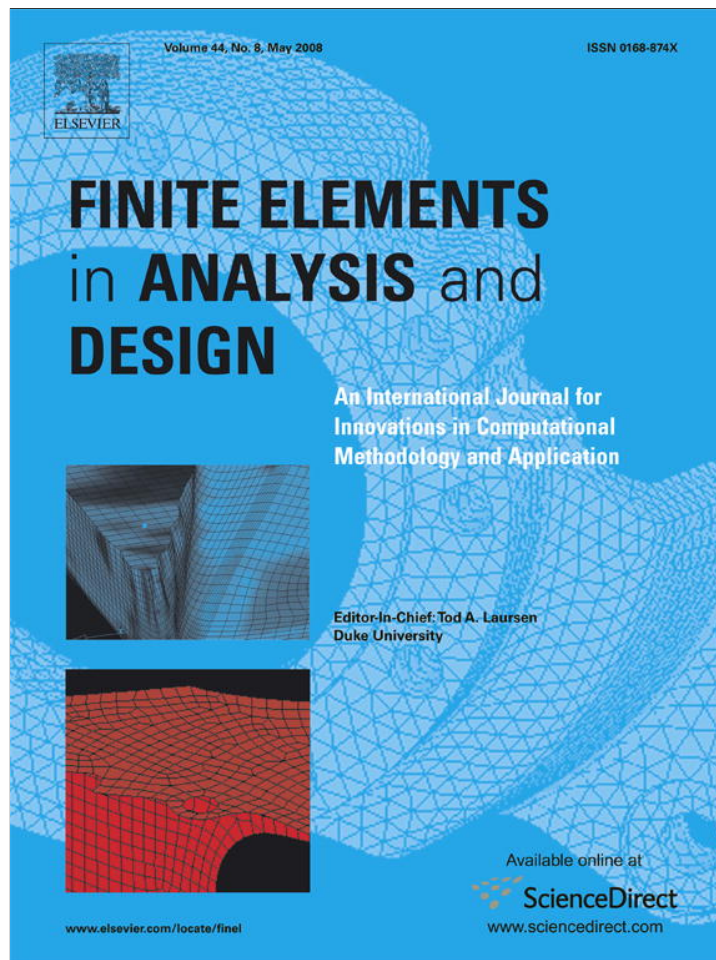


Provided for non-commercial research and education use.  
Not for reproduction, distribution or commercial use.



This article appeared in a journal published by Elsevier. The attached copy is furnished to the author for internal non-commercial research and education use, including for instruction at the authors institution and sharing with colleagues.

Other uses, including reproduction and distribution, or selling or licensing copies, or posting to personal, institutional or third party websites are prohibited.

In most cases authors are permitted to post their version of the article (e.g. in Word or Tex form) to their personal website or institutional repository. Authors requiring further information regarding Elsevier's archiving and manuscript policies are encouraged to visit:

<http://www.elsevier.com/copyright>



ELSEVIER

Available online at [www.sciencedirect.com](http://www.sciencedirect.com)

Finite Elements in Analysis and Design 44 (2008) 513–523

---



---

**FINITE ELEMENTS  
IN ANALYSIS  
AND DESIGN**


---



---

[www.elsevier.com/locate/finel](http://www.elsevier.com/locate/finel)

# Optimization of the static and dynamic characteristics of plates with isogrid stiffeners

W. Akl<sup>a</sup>, A. El-Sabbagh<sup>a</sup>, A. Baz<sup>b,\*</sup><sup>a</sup>*Design and Production Engineering Department, Faculty of Engineering, Ain Shams University, Cairo, Egypt*<sup>b</sup>*Mechanical Engineering Department, University of Maryland, College Park, MD 20742, USA*

Received 9 July 2007; received in revised form 7 January 2008; accepted 7 January 2008

Available online 7 March 2008

---

## Abstract

In this paper, the orientation angles of stiffeners arranged in the form of isogrid configuration over a flat plate are selected to optimize the static and dynamic characteristics of these plates/stiffeners assemblies. The static characteristics are optimized by maximizing the critical buckling loads of the isogrid plate, while the dynamic characteristics are optimized by maximizing multiple natural frequencies of the stiffened plate.

A finite element model is developed to describe the statics and dynamics of Mindlin plates which are stiffened with arbitrarily oriented stiffeners. The model is used as a basis for optimizing separately or simultaneously the critical buckling loads and natural frequencies of the plates per unit volume of the plates/stiffeners assemblies.

Numerical examples are presented to demonstrate the utility of the developed model and optimization procedures. The presented approach can be invaluable in the design of plates with isogrid stiffeners for various vibration and noise control applications.

© 2008 Elsevier B.V. All rights reserved.

*Keywords:* Optimization; Isogrid stiffeners; Stiffened plates; Critical buckling loads; Natural frequency

---

## 1. Introduction

Stiffened plate or shell structures are widely applied in the automobile, aerospace, and ship industries, not to mention in civil constructions. These structures usually consist of a base structure forming the “skin” and local reinforcement elements called “stiffeners” to improve the static and dynamic characteristics of the base structure.

Isogrid stiffener configuration is a special class of stiffened or grid structures whereby the grid members are arranged in an isosceles triangular patterns. Due to their efficiency, these isogrid members have been widely used in many structural applications especially in spacecraft components [1,2]. Analysis of the performance of isogrid structures can be traced back to the work of Slysh et al. [3]. Since then extensive efforts have been exerted to study isogrid structures in an attempt to maximize their stiffnesses, eigenfrequencies, and/or critical buckling loads while imposing stringent constraints on the total

structural mass. Examples of these efforts include the work of Ambur and Rehfield [4] who studied the effect of stiffness discontinuities and structural parameters on the buckling resistance of isogrid panels subject to different loading conditions. It was shown that the nonsolid grid stiffened panels are structurally very efficient for wing and fuselage applications. Also, Huybrechts and Tsai [5] used 3-noded plate finite element model to analyze the behavior of grid structures by predicting the stability and failure of the stiffeners in an attempt to quantify the grid structure strength and the effect of missing ribs. Other researchers have investigated the use of grid structures to enhance the buckling resistance whether by raising the critical load [6,7] or by studying the postbuckled behavior of the isogrid shell [8]. Gan et al. [9] studied the energy absorption in isogrid structures under quasi-static conditions. Under three-point bending loading, Gan et al. showed that isogrid polypropylene panels have excellent damage tolerance. Less attention was paid to studying the behavior of grid structures under dynamic loading conditions. Chen and Gibson [10] used a 3D finite element model with brick elements, for both the skin and the ribs, to predict the modal frequencies and damping factors of isogrid

---

\* Corresponding author. Tel.: +1 301 405 5216; fax: +1 301 405 8331.  
E-mail address: [baz@eng.umd.edu](mailto:baz@eng.umd.edu) (A. Baz).

Nomenclature			
$b$	width of the stiffener	$w, w_b$	displacement in the $z$ -direction of the plate and stiffener elements, respectively
$E$	Young's modulus	$\{\varepsilon_p\}, \{\varepsilon_b\}$	strain vectors in the base plate and stiffener elements, respectively
$G$	shear modulus	$\xi, \eta$	mapping coordinates of the base plate
$h, h_s$	thickness of the skin and stiffener	$\xi', \eta'$	mapping coordinates of the stiffener
$k$	shear factor	$\theta_x, \theta_y, \theta_b$	rotations about the $y$ -, $x$ - and $t$ -axes, respectively
$[\mathbf{K}_b], [\mathbf{K}_p], [\mathbf{K}_E]$	stiffness matrices of the stiffener, base plate, and plate/stiffener assembly, respectively	$\rho_p$	density of the base plate material
$[\mathbf{K}_G]$	geometric stiffness matrix of the plate/stiffener assembly	$\rho_b$	density of the stiffener material
$[\mathbf{M}_b], [\mathbf{M}_p]$	mass matrices of the stiffener and base plate, respectively	$\{\sigma_p\}, \{\sigma_b\}$	stress vectors acting on the base plate and stiffener elements, respectively
$N_x, N_y, N_s$	normal stresses in the $x$ -, $y$ - and $s$ -directions, respectively	$\sigma_x, \sigma_y, \sigma_s$	bending moments in the $x$ -, $y$ - and $s$ -directions, respectively
$N_{xy}$	in-plane $x$ - $y$ torsional stress	$\sigma_{xy}$	out-of-plane ( $x$ - $z$ ) and ( $y$ - $z$ ) torsional stress
$P_{cr}$	critical buckling load	$\tau_x, \tau_y, \tau_s$	shear stresses in the $y$ - $z$ , $x$ - $z$ , $t$ - $z$ faces, respectively
$u, u_b$	displacement in the $x$ -direction of the plate and stiffener elements, respectively	$\{\delta_p\}, \{\delta_b\}$	degrees of freedom of the base plate and stiffener elements, respectively
$v, v_b$	displacement in the $y$ -direction of the plate and stiffener elements, respectively	$\nu$	Poisson's ratio
$V$	element volume	$\phi$	stiffener inclination angle in mapped coordinate system

polypropylene panels with embedded viscoelastic damping layers. Experimentally, the panels were subjected to an impulse excitation. The predictions of the model were validated experimentally.

In general, grid structures have been used in numerous applications. Most of the previous work has been directed to the study of static and buckling characteristics of grid structures. Very few articles discuss their performance in dynamic loading which may lead to a wide implementation in the field of vibration and noise control. Most of the modeling effort was not well suited to these specific structures which resulted in either oversimplified models dealing with the skin and the stiffeners as two independent problems or computationally intensive models with numerous 3D elements. A theoretical model that is able to accurately describe grid structures, without being too complicated to solve, is essential to design topologically optimized grid structures.

Different attempts for maximizing a single or multiple eigenfrequencies of a plate using different topology optimization algorithms have been reported in the literature [11–13]. A common criterion in all these attempts is to reach the best material distribution in plate structures with limited volume. This is usually achieved by modifying the thickness of each element of a finite element mesh of the plate structure independently to maximize the plate eigenfrequencies while satisfying a constraint imposed on the total plate volume. Another approach adopted by Ding and Yamazaki [14] is to implement a topology optimization method for generating stiffener layout patterns by introducing a growing and branching tree model.

Cheng and Olhoff [15] searched for optimal stiffener layout that maximizes the stiffness of rectangular and axisymmetric plates based on an optimal thickness distribution approach. Bendsoe and Kikuchi [16] utilized the well-known homogenization method to analyze composites with perforated microstructures, which are of continuously varying density and orientation, and produced gray-scaled structures using topology optimization. Diaz and Kikuchi [17] considered the problem of optimal reinforcement of plates to increase the fundamental frequency by adding a prescribed amount of reinforcement material. Luo and Gea [18] introduced an optimal bead orientation problem of 3D shell/plate structures for both static and dynamic cases. Using an orthotropic shell design cell model, the optimal bead orientation problem is converted to an optimal orientation problem of bending equivalent orthotropic materials, and it is solved by a new energy-based method. Krog and Olhoff [19] studied the topology optimization problem of statically loaded and freely vibrating disk and plate structures with different types of rib-reinforcement. Buhl et al. [20] extended the homogenization method to the area of geometrically nonlinear structures.

Nevertheless, the problem of optimizing the orientation of the isogrid stiffeners to maximize simultaneously the critical buckling loads and natural frequencies of the plates per unit volume is yet to be tackled. Addressing such a problem is the main objective of the present study.

In this paper, a thick plate model with arbitrary-oriented isogrid stiffeners is considered. The plate is modeled using an 8-node isoparametric element which is formulated using the first-order shear deformation theory. The stiffeners are in turn

modeled using a 3-node element based on the Timoshenko beam theory. Any numbers of stiffeners are allowed to take any arbitrary orientation within the plate element. Constraining the design to be of isogrid nature establishes the foundation for further analysis and synthesis of structures with periodic isogrid stiffeners because of their unique band gap characteristics.

## 2. Finite element model

In this section, an efficient finite element model is developed to accurately model the stiffness and mass matrices of stiffened plates with arbitrarily oriented stiffeners which are generally not distributed in the conventional regular orthogonal arrangements. This capability is essential for the development of a general topology optimization approach of stiffened plates.

Conventionally, stiffened plate structures are divided into small number of finite elements to ensure that the stiffeners are oriented along the boundaries of these elements. This results in a dramatic increase in the number of elements as the number of stiffeners with different orientations and/or small spacing increases. Also, the elements themselves become no longer identical which requires the use of different Jacobean transformation for all the non-identical elements. In addition, the model may require a mix of quadrilateral and triangular elements to satisfy the stiffener-on-the-boundary constraint.

Considering the major drawbacks of the first approach, a finite element model capable of modeling arbitrary-oriented stiffened plates is implemented in this study.

### 2.1. Plate element formulation

#### 2.1.1. Stiffness matrix due to in-plane and bending strains

The stiffness matrix is given by

$$[\mathbf{K}_p] = \int_V \{\boldsymbol{\sigma}_p\}^T \cdot \{\boldsymbol{\epsilon}_p\} dV, \quad (1)$$

where  $\{\boldsymbol{\sigma}_p\} = [\mathbf{D}_p]\{\boldsymbol{\epsilon}_p\}$  is the combined in-plane and bending ( $8 \times 1$ ) stress vector for the plate, as illustrated in Fig. 1 and is defined as

$$\{\boldsymbol{\sigma}_p\} = \{N_x \ N_y \ N_{xy} \ \sigma_x \ \sigma_y \ \sigma_{xy} \ \tau_x \ \tau_y\}^T \quad (2)$$

where  $N_{x,y}$  are normal stresses in the  $x$  and  $y$  directions,  $N_{xy}$  is the in-plane ( $x$ - $y$ ) torsional stress,  $\sigma_{x,y}$  is the bending moment in the  $x$  and  $y$  directions,  $\sigma_{xy}$  is the out of plane ( $x$ - $z$ ) and ( $y$  -  $z$ ) torsional stress,  $\tau_x$  is the shear stress on the  $y$ - $z$  faces, and  $\tau_y$  is the shear stress on the  $x$ - $z$  faces.

Also,  $\{\boldsymbol{\epsilon}_p\}$  denotes the combined in-plane and bending ( $8 \times 1$ ) strain vector for the plate and is defined as

$$\{\boldsymbol{\epsilon}_p\} = \left\{ \frac{\partial u}{\partial x} \frac{\partial v}{\partial y} \left( \frac{\partial u}{\partial y} + \frac{\partial v}{\partial x} \right) - \frac{\partial \theta_x}{\partial x} - \frac{\partial \theta_y}{\partial y} - \left( \frac{\partial \theta_x}{\partial y} + \frac{\partial \theta_y}{\partial x} \right) - \left( \frac{\partial w}{\partial x} - \theta_x \right) - \left( \frac{\partial w}{\partial y} - \theta_y \right) \right\}^T. \quad (3)$$

It can be represented in matrix form as  $\{\boldsymbol{\epsilon}_p\} = [\mathbf{B}_p]\{\boldsymbol{\delta}_p\}$ , where  $u$  is the displacement of the mid-plane in the  $x$ -direction,  $v$  is the displacement of the mid-plane in the  $y$ -direction,  $\theta_x$  and  $\theta_y$

are the resultant mid-plane rotations about the  $y$ - and  $x$ -axes, respectively,  $w$  is the out-of-plane displacement of the mid-plane, and  $\{\boldsymbol{\delta}_p\}$  is the nodal deflection vector of the plate =  $\{u \ v \ w \ \theta_x \ \theta_y\}^T$ . Note that subscripts  $x$  and  $y$  indicate differentiation with respect to the  $x$  and  $y$  coordinates.

#### 2.1.2. Strain–displacement relationship

The strain–displacement relationship for 8-node isoparametric element with 5 degrees of freedom per node is defined as follows:

$$\{\boldsymbol{\delta}_p\} = \sum_{i=1}^8 N_i(\xi, \eta) [\mathbf{I}]\{\boldsymbol{\delta}_i\}, \quad (4)$$

where  $N(\xi, \eta)$  are the mapped shape functions,  $[\mathbf{I}]$  is a  $5 \times 5$  Identity matrix, and  $\{\boldsymbol{\delta}_i\}$  is a nodal degrees of freedom vector. The arbitrary 8-node element, which is defined in the  $x$ - $y$  plane, is mapped to the  $\xi$ - $\eta$  plane to become an 8-node quad element, extending from ( $\xi = -1$ ) to ( $\xi = 1$ ) in one direction and from ( $\eta = -1$ ) to ( $\eta = 1$ ) in the other direction.

Hence, the plate stiffness matrix is defined as

$$[\mathbf{K}_p] = \int_V [\mathbf{B}_p^T][\mathbf{D}_p^T][\mathbf{B}_p] dV. \quad (5)$$

#### 2.1.3. Mass matrix due to in-plane, bending and shear strains

Applying Hamilton's principle to the potential and kinetic energies of the skin element, the mass as well as the stiffness matrices can be calculated [21]

$$[\mathbf{M}_p] = \int_V [\mathbf{M}] dV, \quad (6)$$

where

$$[\mathbf{M}] = \rho_p \begin{bmatrix} h & 0 & 0 & 0 & 0 \\ 0 & h & 0 & 0 & 0 \\ 0 & 0 & h & 0 & 0 \\ 0 & 0 & 0 & \frac{h^3}{12} & 0 \\ 0 & 0 & 0 & 0 & \frac{h^3}{12} \end{bmatrix}. \quad (7)$$

## 2.2. Stiffener element formulation

The stiffener is modeled as a 3-node beam element with 3 degrees of freedom per node ( $u_b, w_b, \theta_b$ ) as shown in Fig. 2. The beam model is based on Timoshenko's beam theory, which is valid for relatively thick beams, as it takes into consideration the shear strains within the beam structure. The stiffener will be initially modeled entirely in its local coordinate system ( $s, t$ ) and its dynamic matrices will be calculated in this system. Then it will be mapped to the plate element coordinate system ( $x, y$ ) based on stiffener's location and orientation.

#### 2.2.1. Stiffness matrix due to in-plane and bending strains

The stiffness matrix is given by

$$[\mathbf{K}_b] = \int_V (\{\boldsymbol{\sigma}_b\}^T \{\boldsymbol{\epsilon}_b\}) dV, \quad (8)$$

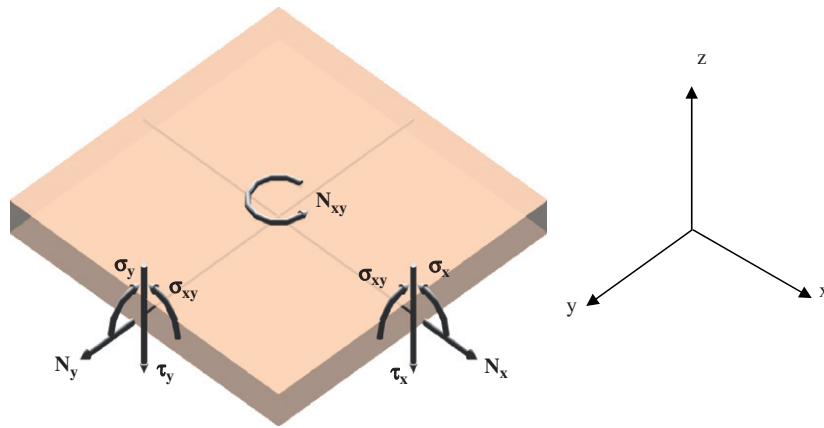


Fig. 1. Stress components acting on a plate element.

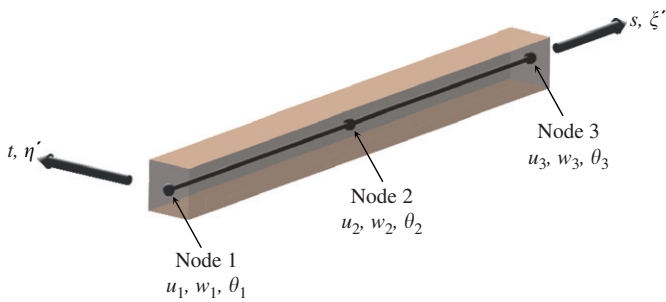


Fig. 2. A 3-node beam element for modeling of the stiffeners in the  $s-t$  coordinate system.

where

$$\{\sigma_b\} = [D_b]\{\epsilon_b\} \quad (9)$$

is the combined in-plane and bending ( $3 \times 1$ ) stress vector for the stiffener and is defined as

$$\{\sigma_b\} = \{N_s \ \sigma_s \ \tau_s\}^T, \quad (10)$$

where  $N_s$  is normal stress in the  $s$ -direction,  $\sigma_s$  is the bending moment in the  $s$ -direction, and  $\tau_s$  is the shear stress on the  $t-z$  faces. Also,  $\{\epsilon_b\}$  is the combined in-plane and bending strain vector of size ( $3 \times 1$ ) for the stiffener and is defined as

$$\{\epsilon_b\} = \left\{ \frac{\partial u_b}{\partial s} \quad -\frac{\partial \theta_b}{\partial s} \quad -\left(\frac{\partial w_b}{\partial s} - \theta_b\right) \right\}^T. \quad (11)$$

It may be represented in matrix form as

$$\{\epsilon_b\} = [B_b]\{\delta_b\} = \begin{bmatrix} \frac{\partial}{\partial s} & 0 & 0 \\ 0 & 0 & -\frac{\partial}{\partial s} \\ 0 & -\frac{\partial}{\partial s} & -1 \end{bmatrix} \begin{Bmatrix} u_b \\ w_b \\ \theta_b \end{Bmatrix}, \quad (12)$$

where  $u$  is the displacement of the mid-plane in the  $x$ -direction,  $\theta_s$  is the mid-plane rotations about the  $t$ -axis,  $w$  is the out-of-plane displacement of the mid-plane, and  $\{\delta_b\}$  is the nodal deflection vector of the plate. Also, subscript ‘S’ indicates

differentiation with respect to the  $s$ -axis and  $[D_b]$  defines the constitutive stress–strain relationship for both the in-plane and bending states and is defined for symmetric stiffener arrangement as

$$[D_b] = \begin{bmatrix} Eh_s & 0 & 0 \\ 0 & \frac{Eh_s^3}{12} & 0 \\ 0 & 0 & Gh_s k \end{bmatrix}, \quad (13)$$

where  $h_s$  is the stiffener thickness.

### 2.2.2. Strain–displacement relationship

The strain–displacement relationship for 3-node beam element with 3 degrees of freedom per node is defined as follows:

$$\{\delta_p\} = \begin{Bmatrix} u_b \\ w_b \\ \theta_b \end{Bmatrix} = \sum_{i=1}^3 N_i(\xi) I \delta_i, \quad (14)$$

where  $N(\xi)$  are the mapped shape functions,  $I$  is a  $3 \times 3$  Identity matrix, and  $\delta_i$  is nodal deflection vector.

The arbitrary 3-node element, which is defined in the  $s-t$  plane along the  $s$ -axis is mapped to the  $\xi'-\eta'$  plane along the  $\xi'$ -axis to become a 3-node element, extending from ( $\xi' = -1$ ) to ( $\xi' = 1$ ).

### 2.2.3. Mass matrix due to in-plane, bending and shear strains

The mass matrix can be calculated from

$$[M_b] = \int_v [M] dv, \quad (15)$$

where

$$[M] = \rho_b b \begin{bmatrix} h_s & 0 & 0 \\ 0 & h_s & 0 \\ 0 & 0 & \frac{h_s^3}{12} \end{bmatrix}. \quad (16)$$

### 2.3. Mapping the stiffener dynamic matrices to the plate coordinate system

The mapping of the stiffener dynamic matrices to the plate coordinate system is achieved in two stages; the first is to map

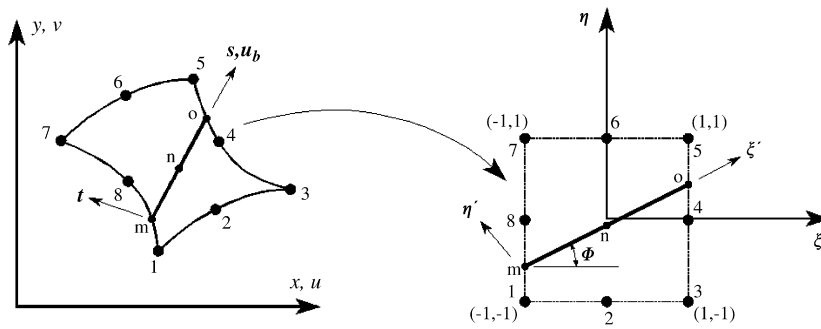


Fig. 3. An 8-node beam element with arbitrary located stiffener.

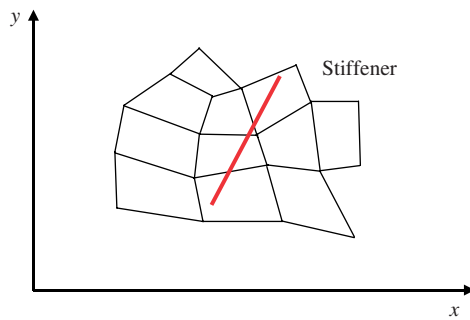


Fig. 4. Inclined stiffener within plate elements.

the matrices to directions parallel to the  $(\xi, \eta)$  coordinate system by using the following transformation:

$$u_b = u \cos(\phi) + v \sin(\phi), \quad \theta_b = \theta_x \cos(\phi) + \theta_y \sin(\phi). \quad (17)$$

This results in the following transformation matrix:

$$\begin{Bmatrix} u_b \\ w_b \\ \theta_b \end{Bmatrix} = \begin{bmatrix} \cos(\phi) & \sin(\phi) & 0 & 0 & 0 \\ 0 & 0 & 1 & 0 & 0 \\ 0 & 0 & 0 & \cos(\phi) & \sin(\phi) \end{bmatrix} \begin{Bmatrix} u \\ v \\ w \\ \theta_x \\ \theta_y \end{Bmatrix}. \quad (18)$$

The second transformation is to map the newly developed stiffness and mass matrices (which now represent the stiffener degrees of freedom defined in the  $\xi$ - $\eta$  coordinate system) to the 8 nodal points of the plate element as shown in Fig. 3. This is achieved by multiplying the stiffener matrices with a transformation matrix that contains the shape functions of the plate element.

Finally, the combined stiffness and geometric stiffness matrices are calculated by adding those of the skin and of the stiffener(s).

Using this approach, stiffeners located arbitrary along a plate structure as in Fig. 4 can be easily modeled without the need to change the ground mesh of the plate model. The only requirement is to calculate the points, where the stiffener intersects the plate element boundaries, and with a simple iteration technique the  $\xi$ - $\eta$  coordinates of these points are calculated.

### 3. Validation of the finite element model

The predictions of the developed finite element model are validated experimentally and against the predictions of a commercial finite element package (ANSYS).

The isogrid plate configuration selected for the validation purposes is shown in Fig. 5. The material of the plate is ABS which is a thermoplastic widely used throughout industry, whose properties are listed in Table 1. The experimental plate is manufactured using stereolithography technique. The dimensions of the plate are given in Table 2.

The experimental plate is fixed in a cantilever configuration, with one edge entirely clamped, leaving the other three edges free to oscillate. The excitation was carried out using a speaker mounted off-center to ensure excitation of all possible modes.

Measurements were done using a scanning laser vibrometer-type Polytec<sup>®</sup> Model (PSV200) to measure the velocity field of the oscillating plates at the modal frequencies. First, a frequency sweep excitation was conducted and the laser measurements were taken at a corner node to determine the natural frequencies. Then surface scans were carried out at the measured natural frequencies. The obtained experimental results were compared with the predictions of ANSYS<sup>®</sup> and the developed model.

Note that the validation of the developed linear finite element model is carried out using a thermo-plastic plate in order to facilitate and reduce the cost of the manufacturing process. The linear model will adequately predict the behavior of the test plate at a constant room temperature which is well below the glass transition temperature of the ABS material. Furthermore,

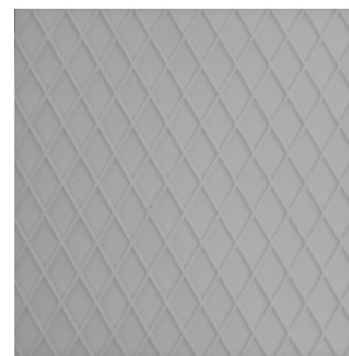


Fig. 5. Configuration of test plate with isogrid stiffeners.

Table 1  
Material properties for ABS

Tensile strength	22 MPa	Tensile modulus	1.627 MPa
Tensile elongation	6%	Specific gravity	1.05

Table 2  
Dimensions of plates in mm (in)

Parameter	Isogrid stiffeners
Width	190 (7.5)
Length	198 (7.5)
Skin thickness	1.6 ( $\frac{1}{16}$ )
Stiffener thickness	1.6 ( $\frac{1}{16}$ )
Stiffener width	1.6 ( $\frac{1}{16}$ )

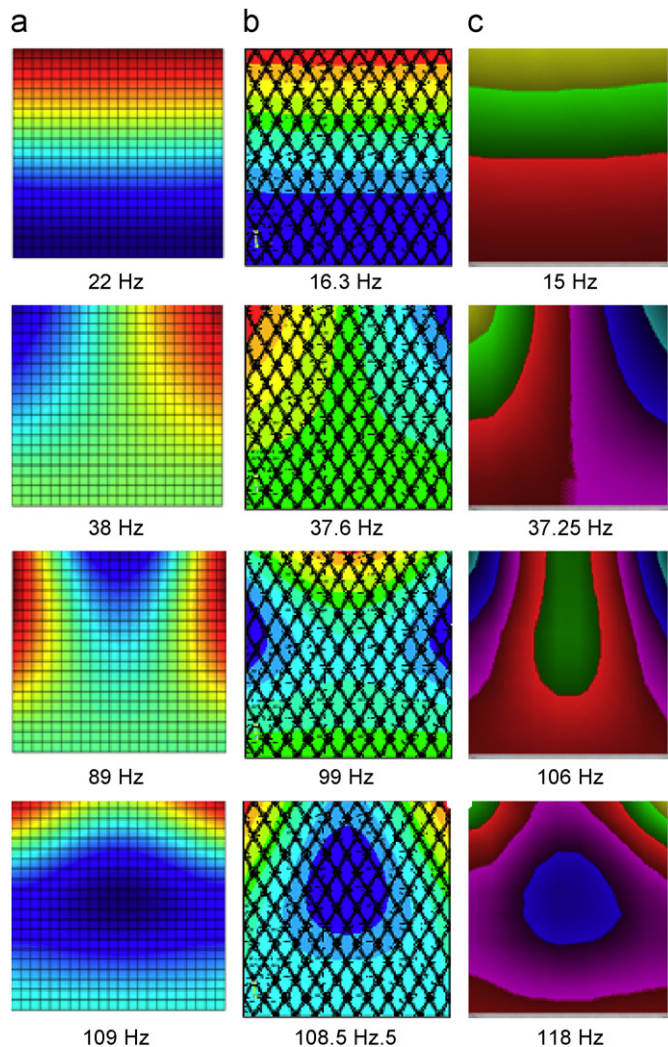


Fig. 6. First four mode shapes for plate with isogrid stiffeners as predicted by (a) the developed model, (b) ANSYS®, and (c) experimentally measured.

the excitation of the plate dynamics is maintained low in order to avoid large amplitudes of oscillations that may render the dynamics to be nonlinear.

Fig. 6 shows the first four mode shapes for the isogrid plates. In the figure, the left column (a) is for the modes predicted by

the proposed model, the middle column (b) is for those predicted by ANSYS®, while the right column (c) is for those experimentally measured modes. Very good matching can be observed for the theoretical predictions and experimental results. Also, the matching between the predictions of the proposed model, which uses the new plate elements, and those of ANSYS®, which uses the conventional plate elements, is very good, taking into consideration that the proposed model uses only 110 elements for the isogrid plate for instance compared with 7432 elements used by ANSYS®.

#### 4. Optimization of the static and dynamic characteristics

##### 4.1. Critical buckling loads

To calculate the critical stability condition or in other words the critical value  $P_{cr}$  of the in-plane loads at which buckling starts to occur, the following eigenvalue problem should be solved:

$$[\mathbf{K}_E] - P_{cr}[\mathbf{K}_G] = 0, \tag{19}$$

where  $[\mathbf{K}_E]$  and  $[\mathbf{K}_G]$  are the overall and the geometric stiffness matrices for the plate/stiffener system.

##### 4.2. Optimization of buckling loads

The objective here is to find the inclination angle  $\phi$  for the symmetric stiffener arrangements that maximizes the critical buckling load per unit volume of the stiffened plate structure which is defined as the “specific critical buckling load”.

Hence, the optimization formulation takes the following form:

$$\left\{ \begin{array}{l} \max_{\phi} \sum_{i=1}^N \frac{P_{cr_i}(\phi)}{V} = \text{specific critical buckling load} \\ \text{such that: } \mathbf{K}_E - P_{cr_i} \mathbf{K}_G = 0, \\ V = V(\phi), \\ 0 \leq \phi \leq \frac{\pi}{2}, \\ N = \text{number of considered critical buckling loads} \end{array} \right. \tag{20}$$

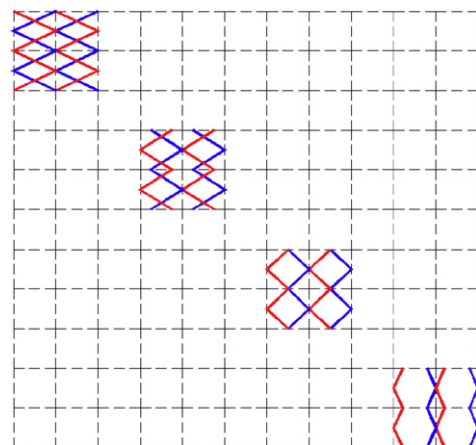


Fig. 7. Samples of the stiffeners orientation within the plate.

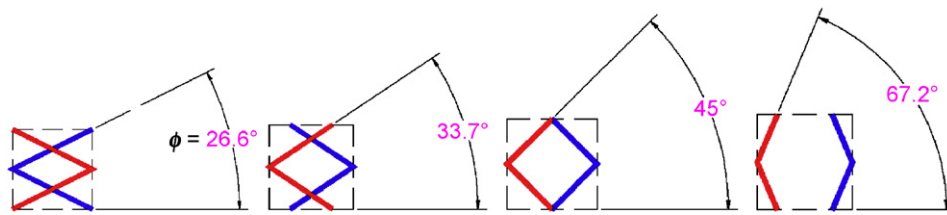


Fig. 8. Definition of the stiffener inclination angle.

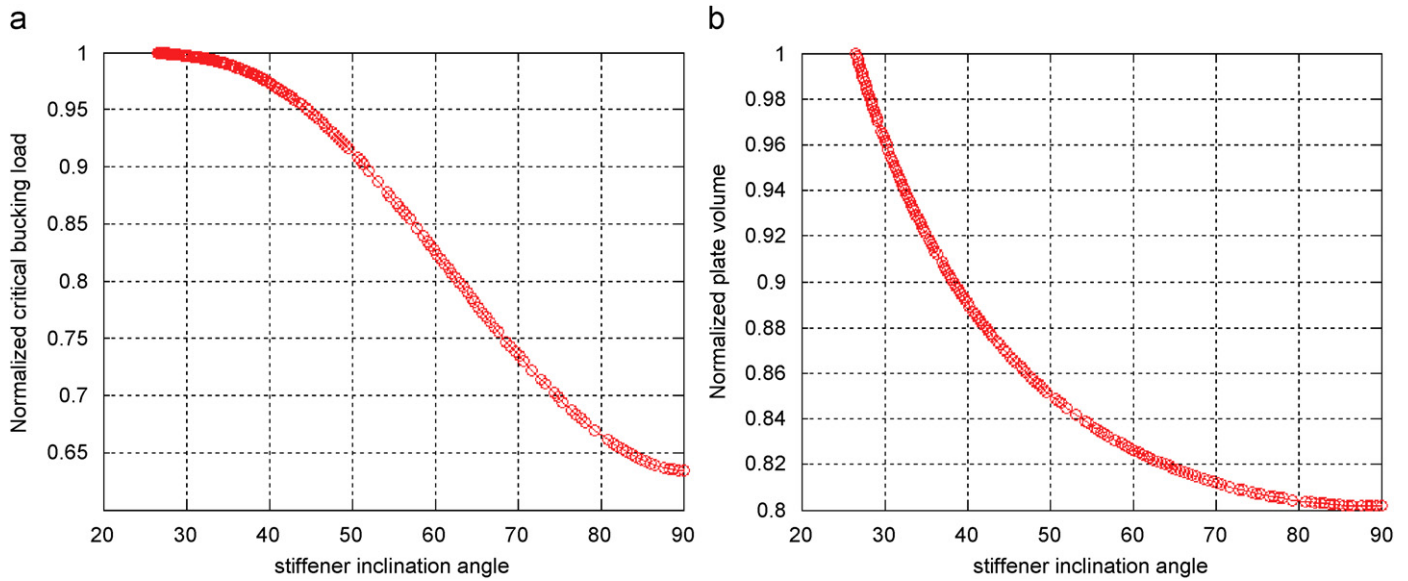


Fig. 9. Normalized first critical buckling load (a) and normalized plate volume (b).

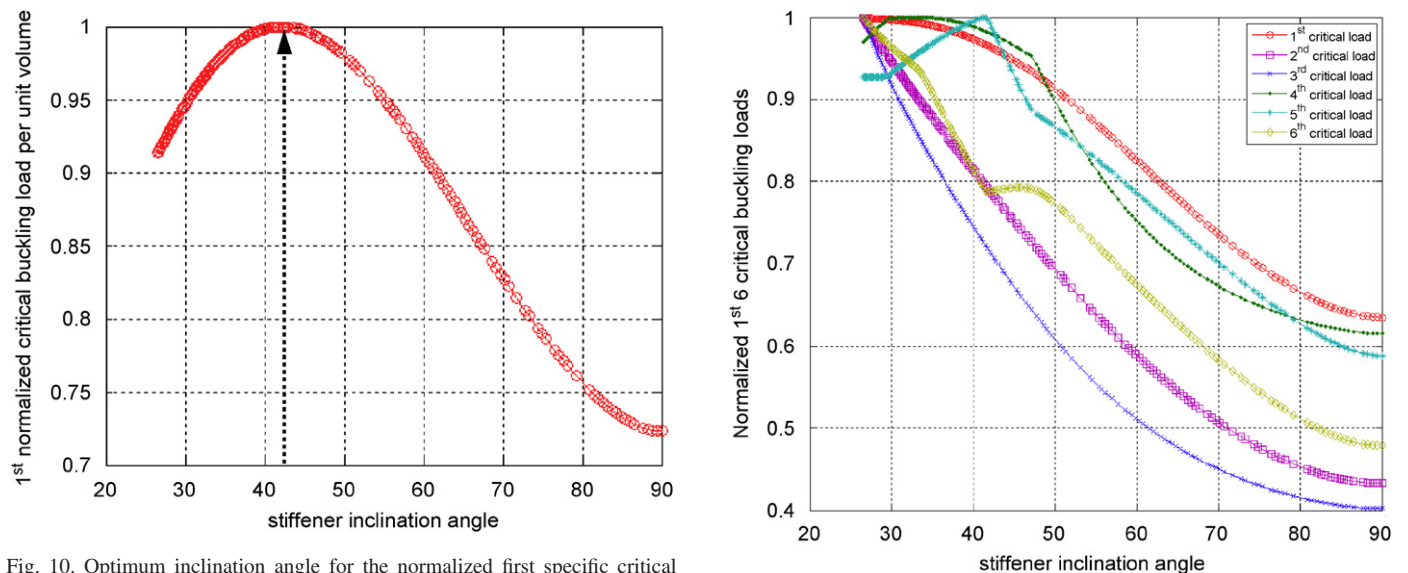


Fig. 10. Optimum inclination angle for the normalized first specific critical buckling load.

Fig. 11. Normalized first six critical buckling loads.

The optimization problem is solved while taking the following into consideration:

1. The plate structure is of cellular form as illustrated in Fig. 7.
2. Four stiffeners are attached to each cell of the plate structure.

3. The design variable is the inclination angle  $\phi$  of the stiffeners. Fig. 8 illustrates four arrangements of the stiffeners as obtained for four different values of the angle  $\phi$ .
4. The plate under investigation is square and clamped from all edges with skin thickness and stiffener thickness and

width of  $\frac{1}{16}$  in. The plate width is 7.5 in and is made of a thermoplastic material (ABS) with  $E = 1.627$  MPa and  $\rho = 1050$  kg/m<sup>3</sup>.

- All data are presented in a normalized form, which is calculated by dividing the different function values (buckling load or plate volume) by their maximum value.

The normalized first critical buckling load and the normalized plate volume as a function of the stiffener inclination angle are calculated and plotted in Figs. 9(a) and (b), respectively.

By calculating the first critical buckling load per unit volume and plotting it for different values of stiffener inclination angles as shown in Fig. 10, an optimum value for inclination angle of 42° was found to maximize the first critical buckling load while taking the plate volume, and consequently, its weight into consideration.

Extending the analysis to maximize the first six critical buckling loads results in a different optimum stiffener inclination angle of 35° as shown in Figs. 11 and 12

Note that the discontinuities in the plots of the first six critical buckling loads (Fig. 11) are a result of ranking the loads in

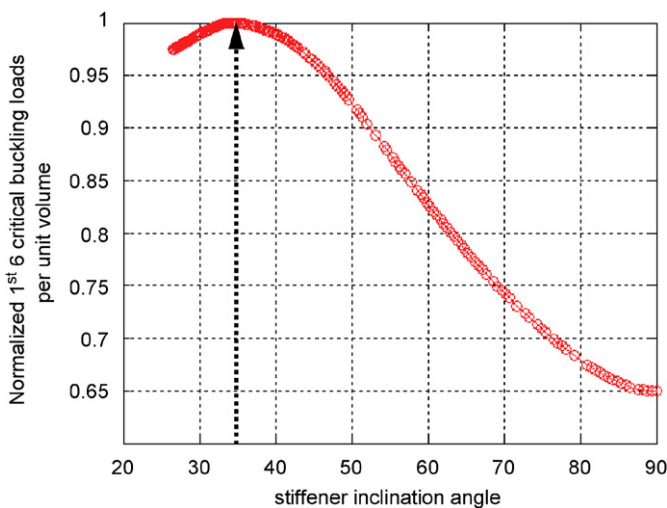


Fig. 12. Optimum inclination angle for the normalized first six critical buckling loads.

an ascending order without considering their associated mode shapes. Such a ranking procedure is essential to compute the “specific critical buckling loads” which is given by

$$\sum_{i=1}^N \frac{P_{cr_i}}{V}$$

Figs. 13(a) and (b) illustrate the shapes of the stiffened plate that maximize the fundamental specific frequency and the first six specific critical buckling loads, respectively.

### 4.3. Natural frequencies

To calculate the natural frequencies of the entire plate/stiffeners structure, the following eigenvalue problem should be solved:

$$[\mathbf{K}] - \lambda_i [\mathbf{M}] = 0, \tag{21}$$

where  $[\mathbf{K}]$  and  $[\mathbf{M}]$  are the overall stiffness and mass matrices for the entire structure, respectively, and  $\lambda_i = \omega_i^2$  is the  $i$ th eigenvalue.

### 4.4. Optimization of the natural frequencies

The objective here is to find the inclination angle  $\phi$  for the symmetric stiffener arrangements that maximizes the natural frequency per unit volume of the stiffened plate structure, which is defined as the “specific natural frequency”.

Hence, the optimization formulation takes the following form:

$$\left\{ \begin{array}{l} \max_{\phi} \sum_{i=1}^N \frac{\lambda_i(\phi)}{V} = \text{specific natural frequency} \\ \text{such that: } \mathbf{K} - \lambda_i \mathbf{M} = 0, \\ V = V(\phi), \\ 0 \leq \phi \leq \frac{\pi}{2}, \\ N = \text{number of considered natural frequencies} \end{array} \right. \tag{22}$$

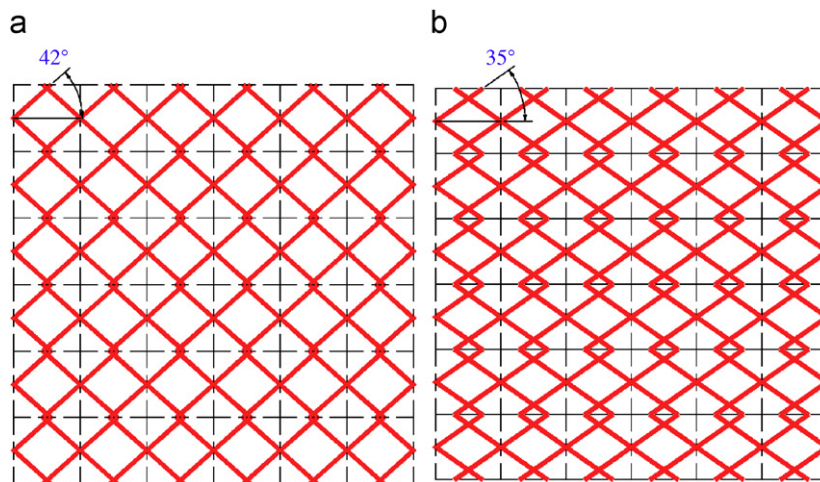


Fig. 13. Stiffeners configurations that maximize the first specific critical buckling load (a) and the first six specific critical buckling loads (b).

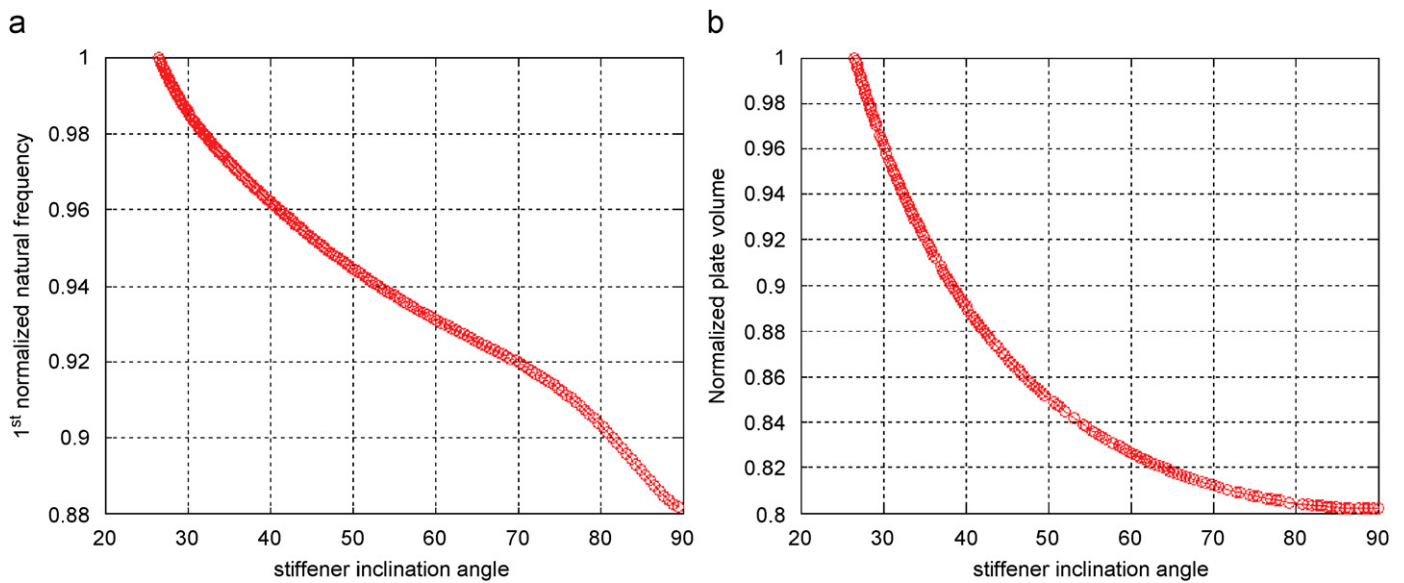


Fig. 14. Normalized first natural frequency (a) and normalized plate volume (b).

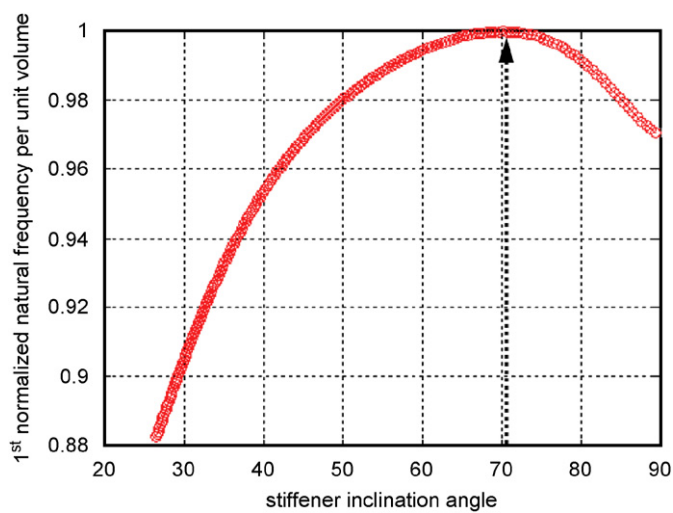


Fig. 15. Optimum inclination angle for the normalized first specific natural frequency.

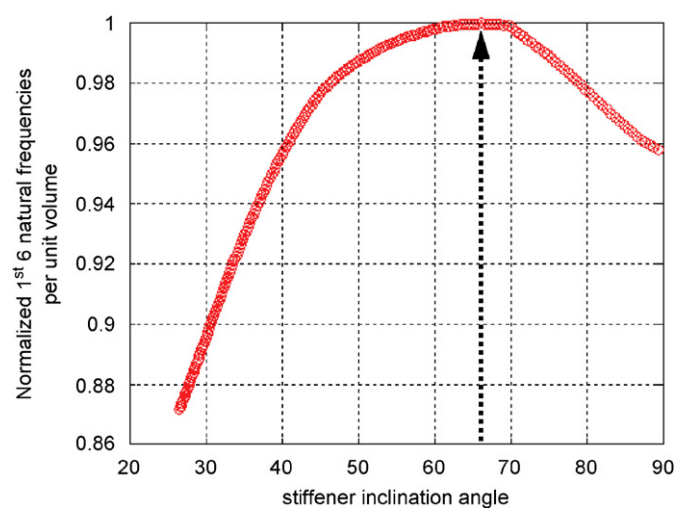


Fig. 17. Optimum inclination angle for the normalized first six natural frequencies.

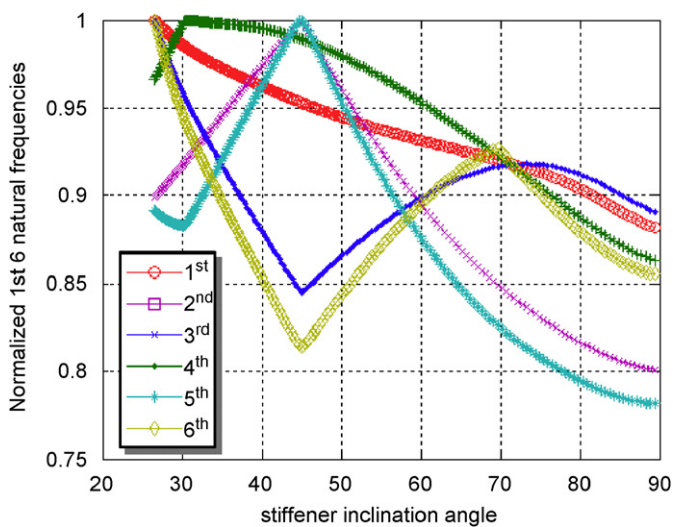


Fig. 16. Normalized first six natural frequencies.

The normalized first natural frequency ( $N = 1$ ) and the normalized plate volume as a function of the stiffener inclination angle are calculated and plotted in Figs. 14(a) and (b), respectively.

By calculating the fundamental natural frequency per unit volume and plotting it for different values of stiffener inclination angles as shown in Fig. 15, an optimum value for inclination angle of 70.5° was found to maximize the fundamental frequency, taking the plate volume and, consequently, its weight into consideration.

Extending the analysis to account for the first six natural frequencies ( $N = 6$ ) results in an optimal stiffener inclination angle of 66.5° as shown in Figs. 16 and 17.

Note that the discontinuities in the plots of the first six natural frequencies (Fig. 16) are a result of ranking the frequencies in an ascending order without considering their associated mode shapes. Such a ranking procedure is essential to compute

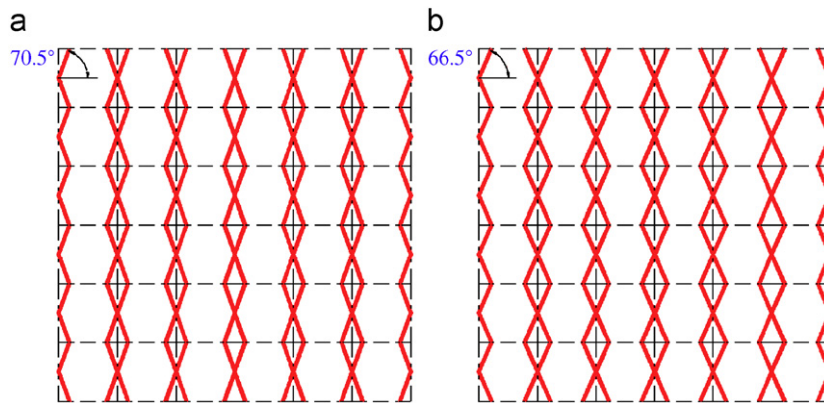


Fig. 18. Stiffeners configurations that maximize the first specific natural frequency (a) and the first six specific natural frequencies (b).

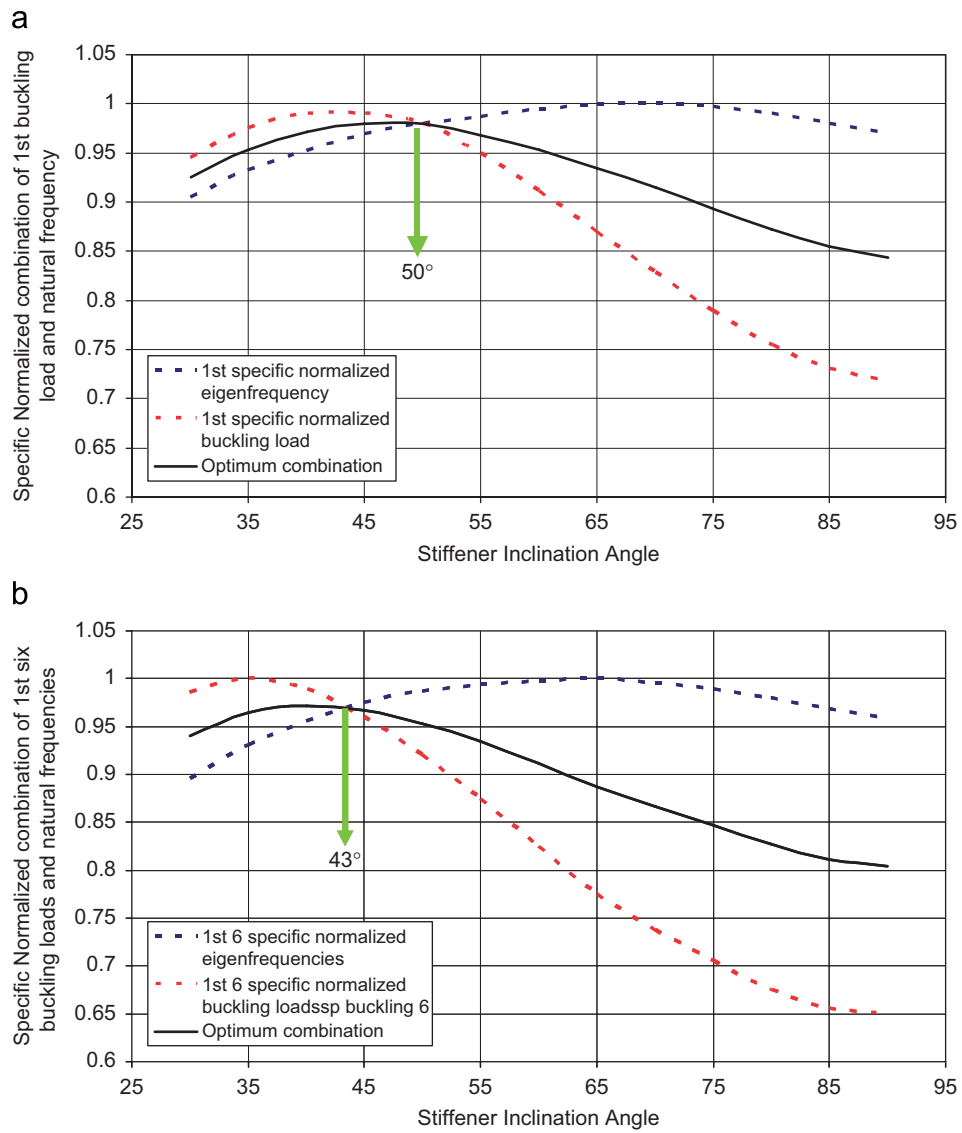


Fig. 19. Multi-objective optimization for first buckling load and natural frequency (a) and for first six buckling loads and natural frequencies (b).

the “specific natural frequencies” which is given by

$$\sum_{i=1}^N \frac{\lambda_i(\phi)}{V}$$

Figs. 18(a) and (b) illustrate the resulting shape of the stiffened plate that maximizes the fundamental specific frequency and the first six specific natural frequencies, respectively.

#### 4.5. Multi-objective optimization of buckling loads and natural frequencies

The optimization problem is formulated as follows:

$$\left\{ \begin{array}{l} \max_{\phi} \sum_{i=1}^N \left( \frac{P_{cr_i}}{V} + \frac{\lambda_i(\phi)}{V} \right) \\ \text{such that: } \mathbf{K} - \lambda_i \mathbf{M} = 0, \\ \mathbf{K}_E - P_{cr_i} \mathbf{K}_E = 0, \\ V = V(\phi), \\ 0 \leq \phi \leq \frac{\pi}{2}, \\ N = \text{number of considered buckling} \\ \text{loads and natural frequencies} \end{array} \right. \quad (23)$$

Figs. 19(a) and (b) show the optimal orientation angles for  $N=1$  and 6, respectively.

### 5. Conclusions

This paper has presented a rational design approach to optimize the static and dynamic characteristics of plates stiffened with isogrid stiffeners. The optimal orientation angles of the stiffeners are selected in order to optimize, separately or simultaneously, the static characteristics as measured by the critical buckling loads and dynamic behavior as quantified by the natural frequencies. For the configurations considered, it has been shown that maximizing the first critical buckling load/unit volume requires the orientation angles of the stiffeners to be  $42^\circ$ . These angles become  $35^\circ$  when maximizing the first six critical buckling loads/unit volume. For maximizing the first natural frequency/unit volume, the optimal orientation angles are found to be equal to  $70.5^\circ$  and  $66.5^\circ$  when one maximizes the first six specific natural frequencies. Simultaneous optimization of the buckling and the natural frequencies results in orientation angles of  $50^\circ$  and  $43^\circ$  for the first modes and for the first six modes, respectively.

The presented finite element model and optimization procedures will be extended to the study of the band gap characteristics of such a class of plates with periodic isogrid stiffeners. Such a study will be invaluable in controlling the propagation of waves over this class of 2D structures both in the spectral and spatial domains.

### Acknowledgments

This work is funded by the Office of Naval Research (Grant number N000140610074). Special thanks are due to Dr. Kam Ng, the technical monitor, for his invaluable inputs.

### References

- [1] E. Silverman, M. Rhodes, M. Dyer, Composite isogrid structures for spacecraft components, SAMPE J. 35 (1999) 51–59.
- [2] S. Huybrechts, T. Meink, Advanced grid stiffened structures for the next generation of launch vehicles, IEEE Aerosp. Appl. Conf. Proc. 1 (1997) 263–269.
- [3] P. Slyph, J. Dyer, J. Furman, J. Key, Isogrid structural tests and stability analyses, J. Aircr. 13 (1976) 778–785.
- [4] D. Ambur, L. Rehfield, Effect of stiffness characteristics on the response of composite grid-stiffened structures, J. Aircr. 30 (1993) 541–546.
- [5] S. Huybrechts, S. Tsai, Analysis and behavior of grid structures, Compos. Sci. Technol. 56 (1996) 1001–1015.
- [6] S. Anderson, Buckling of periodic structures, in: Collection of Technical Papers—AIAA/ASME/ASCE/AHS Structures, Structural Dynamics & Materials Conference, 1980, 159–166.
- [7] E. Wodesenbet, S. Kidane, S. Pang, Optimization for buckling loads of grid stiffened composite panels, Compos. Struct. 60 (2003) 159–169.
- [8] D. Kim, Postbuckled behavior of composite isogrid stiffened shell structure, Adv. Compos. Mater. Off. J. Japan Soc. Compos. Mater. 9 (2000) 253–263.
- [9] C. Gan, R. Gibson, G. Newaz, Analytical/experimental investigation of energy absorption in grid-stiffened composite structures under transverse loading, Exp. Mech. 44 (2003) 185–194.
- [10] Y. Chen, R. Gibson, Analytical and experimental studies of composite isogrid structures with integral passive damping, Mech. Adv. Mater. Struct. 10 (2003) 127–143.
- [11] M.P. Bendsoe, O. Sigmund, Topology Optimization Theory, Methods and Applications, Springer, Germany, 2003.
- [12] N.L. Pedersen, Maximization of eigenvalues using topology optimization, Struct. Multidisciplinary Optim. 20 (2000) 2–11.
- [13] J. Du, N. Olhoff, Topology optimization of continuum structures with respect to simple and multiple eigenfrequencies, in: 6th World Congresses of Structural and Multidisciplinary Optimization, Rio de Janeiro, Brazil, 2005.
- [14] X. Ding, K. Yamazaki, Stiffener layout design for plate structures by growing and branching tree model (application to vibration-proof design), Struct. Multidisciplinary Optim. 96 (2004) 99–110.
- [15] K.T. Cheng, N. Olhoff, An investigation concerning optimal design of solid elastic plates, Int. J. Solids Struct. 17 (1981) 305–323.
- [16] M.P. Bendsoe, N. Kikuchi, Generating optimal topologies in structural design using a homogenization method, Comput. Methods Appl. Mech. Eng. 71 (1988) 197–224.
- [17] A.R. Diaz, N. Kikuchi, Solution to shape and topology eigenvalue optimization problems using a homogenization method, Int. J. Numer. Methods Eng. 35 (1992) 1487–1502.
- [18] G.H. Luo, H.C. Gea, Optimal bead orientation of 3D shell/plate structures, Finite Elem. Anal. Design 31 (1998) 55–71.
- [19] L.A. Krog, N. Olhoff, Optimum topology and reinforcement design of disk and plate structures with multiple stiffness and eigenfrequency objectives, Comput. Struct. 72 (1999) 535–563.
- [20] T. Buhl, C.B.W. Pedersen, O. Sigmund, Stiffness design of geometrically nonlinear structures using topology optimization, Struct. Multidisciplinary Optim. 19 (2000) 93–104.
- [21] H. Baruh, Analytical Dynamics, McGraw-Hill, New York, 1999.